ORIGINAL ARTICLE

Novel microneedle patches for transdermal delivery of AP39, a hydrogen sulphide donor, in the treatment of scenarios mimicking neurological disorders

Pavanjeeth Balakrishnan[1] · Sarah Junaid[1] · Shakil Ahmad[2] · Keqing Wang[2] · Yukta Sameer Hindalekar[2] · Hala Shokr[3] · Manoj Upadhya[4] · Sarah Hopkins[2] · Jakub Sacharczuk[5] · Karan Singh Rana[6] · Mohamad Anas Al Tahan[2] · Parag Juvale[4] · Felix Chan[4] · Lissette Sanchez-Aranguren[2] · Mandeep Marwah[2]

Abstract

Purpose Neurodegenerative diseases such as Alzheimer's disease and Parkinson's disease are debilitating conditions resulting from a progressive degeneration of nerve cells that is attributed to oxidative stress. Given the role of hydrogen sulphide (H_2S), an endogenously produced signalling molecule involved in regulating of oxidative stress, exogenous administration of H_2S has been proposed as a potential treatment strategy. This research study involved an investigation into the mechanical properties of microneedles loaded AP39 (a H_2S donor), their ability to penetrate skin and effectiveness to deliver AP39 across murine skin. Additionally, the study explored the capability of permeated AP39 to release H_2S and thus quench H_2O_2-induced oxidative stress in neuroblastoma cells, SHSY5Y cells.

Methods Microneedles were prepared using 20% w/v polyvinyl alcohol (PVA) of either 27,000 or 67,000 molecular weights, with or without trehalose 15% w/v. Mechanical and insertion properties of microneedles were determined and optimised formulation applied to murine skin to observe AP39 flux through the skin. Collected media was applied to a microvasculature blood–brain-barrier model to evidence AP39 permeation, following which, permeated AP39 was applied to an oxidative stress scenario in SHSY5Y cells to assess AP39 potential in limiting oxidative stress.

Results Microneedle fracture testing observed the microneedles produced from polyvinyl alcohol 67,000 with trehalose were best able to withstand compression force applied. Microneedles formulated from PVA 67,000 were best able to penetrate the parafilm model. Further, the PVA 67,000 with trehalose microneedle formulation was observed to pierce murine skin and deliver $32.84 \pm 2.11\%$ of applied AP39 across the skin over 32 h. AP39 transport across the HUVEC microvasculature model gave an apparent membrane permeability of 18.6 ± 1.4. Finally, AP39 attenuated H_2O_2-induced oxidative stress as well as inflammation in SHSY5Y cells; resulting in reduced neurodegeneration burden.

Conclusion These findings demonstrate that microneedle patches for the transdermal delivery of AP39 may provide a promising clinical approach in the treatment of neurological disorder associated with oxidative stress.

Keywords Transdermal drug delivery · Microneedles · Controlled-release · Oxidative stress · Neurodegeneration

✉ Sarah Junaid
s.junaid@aston.ac.uk

✉ Mandeep Marwah
m.marwah1@aston.ac.uk

1 School of Engineering and Technology, College of Engineering and Physical Sciences, Aston University, Birmingham, UK

2 Aston Medical School, College of Health and Life Sciences, Aston University, Birmingham, UK

3 Pharmacy Division, School of Health Sciences, Faculty of Biology, Medicine and Health, The University of Manchester, Manchester, UK

4 Aston Pharmacy School, College of Health and Life Sciences, Aston University, Manchester, UK

5 Aston Institute of Materials Research, Aston University, Manchester, UK

6 School of Biosciences, College of Health and Life Sciences, Aston University, Manchester, UK

Introduction

Neurodegenerative diseases such as Alzheimer's, Parkinson's and Huntington's disease are debilitating conditions characterized by a progressive deterioration and selective impairment of neurons and glial cells within the human brain and spinal cord (Relja 2004). These conditions lead to a progressive decline of cognitive abilities and/or motor skills (Checkoway et al. 2011). A multitude of factors are implicated in the development of neurodegenerative diseases (Dugger and Dickson 2017) with oxidative stress (Singh et al. 2019), neuroinflammation (Amor et al. 2010), mitochondrial dysfunction (Wang et al. 2019), and protein aggregation (Jellinger 2010) listed as primary underlying causes of human neurodegeneration. Mitochondrial reactive oxygen species (ROS) play a significant role in the pathogenesis and progression of neurodegenerative diseases (Kausar et al. 2018) with excessive generation of ROS resulting in a loss of the central nervous system antioxidant pathways resulting in damage to neuronal proteins and nucleic acids (Nissanka and Moraes 2018). Consequently, most of the promising approaches for the prevention and treatment of neurodegenerative diseases involved the utilisation of therapeutic agents that aim to reduce oxidative stress and restore mitochondrial function (Zhao et al. 2016).

Hydrogen sulphide (H_2S), an endogenously produced signalling molecule, has gained attention as a noteworthy neuromodulator and neuroprotective molecule with substantial clinical implications in the central nervous system (Shefa et al. 2018). H_2S has been observed to exhibit its antioxidant properties by scavenging ROS by mediating the activities of glutathione peroxidise, super oxide dismutase and the catalase enzyme in the central nervous system (Zhang and Bian 2014; Tabassum et al. 2020). Thus, H_2S donor molecules may offer a potential therapeutic option in the treatment of neurodegenerative disorders. In fact, studies have shown that treatment with H_2S reduces the loss of substantia nigra neurons and slows down motor dysfunction development in rodent Parkinson's disease models (Hu et al. 2010). Despite the promising outcomes regarding its therapeutic potential, pharmaceutical formulation of H_2S has encountered numerous challenges and limitations, which have hindered its successful translation into clinically approved therapies. H_2S is a small, highly diffusible molecule that can easily cross cell membranes which makes achieving targeted delivery to specific tissues challenging (Caliendo et al. 2010). In light of this context, AP39 has garnered attention as an innovative H_2S donor unique in its ability to specifically target the mitochondria (Szczesny et al. 2014). Studies have demonstrated that AP39 administration can confer neuroprotective effects by mitigating mitochondrial dysfunction, reducing oxidative stress, and modulating cellular signalling pathways in preclinical models of various diseases (Szczesny et al. 2014; Ikeda et al. 2015; Gerő et al. 2016). Nevertheless, the rapid release of H_2S through conventional delivery methods such as intravenous or intraperitoneal routes are inconvenient and pose a risk of toxicity, highlighting the importance of developing safe, controlled-release formulations for delivering these compounds in clinical settings (Teo et al. 2006).

Over recent years, transdermal drug delivery has emerged as a popular method of drug delivery owing to its ease of application and capacity for controlled-drug release (Alkilani et al. 2015). Nonetheless, it faces a significant challenge with the stratum corneum acting as a protective barrier that restricts the penetration of drugs through the skin. To address this, microneedle devices have been employed to enhance the delivery of therapeutics. These devices consist of micron size needles arranged on a small patch, with potential for controlled-drug administration (Alkilani et al. 2015). By creating microscopic channels in the skin, microneedles facilitate improved penetration and absorption of drugs by allowing direct drug contact with the epidermis or upper dermis region, thereby enhancing the bioavailability and effectiveness of the medications (Alkilani et al. 2015). Dissolving microneedle patches are formulated from biocompatible cellulose derivatives along with sugars which increase the mechanical strength of the needles (Kima et al. 2016; Tian et al. 2022). Polyvinyl alcohol (PVA) is one such biopolymer with the mechanical strength to withstand the insertion force whilst being able to rapidly dissolve (Moore et al. 2022). The needles, up to 1 mm in length, do not cause pain with minimal tissue damage (Dabbagh et al. 2021; Jung and Jin 2021). Patches are low cost to manufacture, easy to apply by the patient and can deliver drug over a week thereby reducing healthcare intervention. Considering a limiting factor of H_2S donor compounds is their rapid breakdown in vivo, patches could offer a solution in providing a slow release of H_2S donor (Marwah et al. 2022).

Thus, the main objective of this study was to examine the viability of transdermal microneedles for delivering AP39 and evaluate the efficacy of permeated AP39 in mitigating oxidative stress induced by H_2O_2 in SHSY5Y cells. Furthermore, the mechanical properties of the formulation and delivery system were assessed, along with the rate of dissolution through ex vivo skin and in vitro permeation across a microvasculature blood-brain barrier model.

Materials and methods

Materials

Clear resin V4 was obtained from Formlabs Inc. (Somerville, MA, USA). Polyvinyl siloxane was obtained from R&S (Tremblay, France). PVAs (average molecular weight of 27,000 and 67,000) and trehalose dihydrate were obtained from Sigma-Aldrich (Dorset, UK). AP39 (#17100) was obtained from Cayman Chemical (Ann Arbor, MI, USA). Parafilm M (127 μm thickness) and 1,1'-Di-n-octadecyl-3,3,3',3'-tetramethylindocarbocyanine perchlorate, 97% (DilC) was obtained from ThermoFisher Scientific (Loughborough, UK). VECTASHIELD Antifade Mounting Medium with 4',6-diamidino-2-phenylindole (DAPI) was obtained from Vector Laboratories (Burlingame, CA, USA). All other reagents including acetonitrile, methanol, and acetic acid were obtained from Sigma-Aldrich (Dorset, UK).

Microneedle mould fabrication

Microneedle fabrication was a three-step procedure (El-Sayed et al. 2020) including 3D printing a master mould to create a negative mould in Polyvinyl Siloxane, which was used to produce the final microneedle array. The positive resin mould was designed on Autodesk Fusion 360 version 2.0.14113 (San Rafael, CA, USA) and printed on the Formlabs Form 2 (Somerville, MA, USA) using clear resin V4 at 25 μm layer thickness. The design of the microneedles, based on that by Krieger et al. (Krieger et al. 2019), included needles with a conical shape of 1750 μm height, 312.5 μm base diameter with a microneedle array of 7×7, 950 μm apart, with a needle removed from its 4 corners, resulting in 45 needles (Krieger et al. 2019). The negative mould was a simple construction made by creating an imprint of the positive resin mould into Polyvinyl Siloxane (Fig. 1).

Microneedle fabrication

Microneedles were formulated from PVA 20% w/v of two different molecular weights, either 27,000 or 67,000 either with or without trehalose 15% w/v for comparison. The polymer was added to either water or trehalose solution and left to stir at 90 °C temperature until the polymer dissolved. Microneedles with an AP39 loading of 0.008% w/v were manufactured by adding the required amount of AP39, dissolved in ethanol, to the prepared polymer mix and stirring for 1 h. From this, 500 uL was pipetted into the mould and centrifuged at 2500 rpm for 20 min at 20 °C. Following, the filled moulds were kept at 55 °C for 3 h for dehydration after which, the microneedles were carefully removed. Microneedle-free control patches were prepared by the same method, except using flat moulds with no indentations. Microneedle preparations were assessed with scanning transmission electron microscopy imaging for patch appearance, array uniformity, and needle length. Images were taken using the Environmental Scanning Electron Microscope mode of the ThermoFisher Scientific Quattro S microscope equipped with a field emission filament. The images were taken in Low Vacuum Detection mode in a variable pressure of 95 Pa, with an acceleration voltage of 15 kV and spot size of 3.

Mechanical and insertion properties of AP39 loaded MN arrays

The mechanical strength of the microneedles was determined with fracture testing (Thakur et al. 2016). Briefly, the microneedle array was fixed to the moving crosshead of the TA Electroforce 3200 using double sided 3 M tape. This was to simulate the skin insertion technique (Supplementary Fig. 1). The microneedles were compressed at a rate of 0.01 mm/s until a 32 N load was achieved. This load was then held for 30 s, and then released at a rate of 0.1 mm/s.
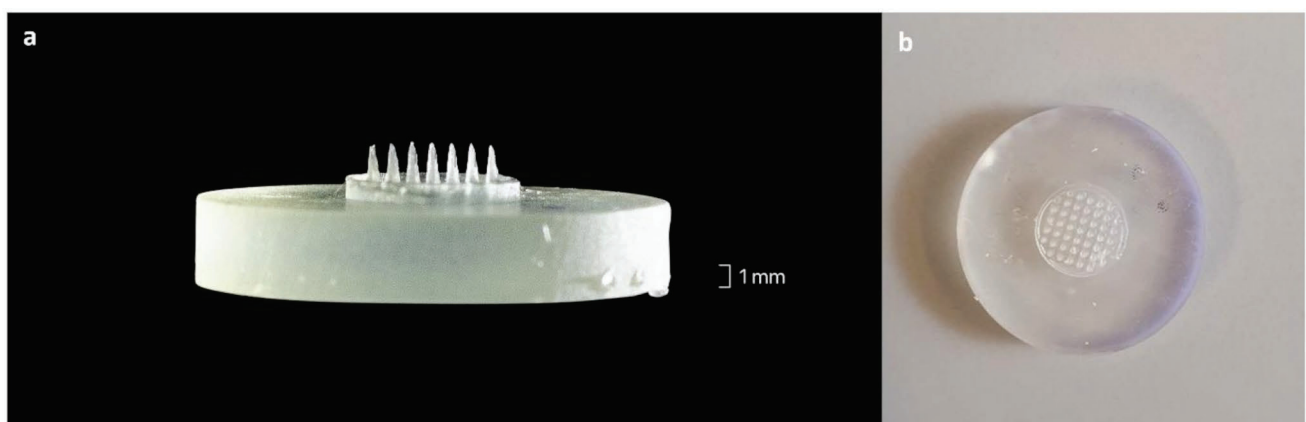

Fig. 1 Positive resin microneedle mould printed by Formlabs Form 2 using clear resin V4 (**a**) side view and (**b**) top view

The load force and displacement were recorded at a rate of 20 readings per second. Data was used to calculate initial break force, stiffness and holding displacement.

To determine insertion/penetration properties of the microneedles, Parafilm M® was used as per a previously validated model (Vora et al. 2017). Briefly, the microneedle array was attached to the moving crosshead using double sided 3 M tape of the TA Electroforce 3200. On the opposing side, 8 layers of 0.12 mm thick parafilm was fixed in place to test. The microneedles were then inserted into the parafilm layers at a rate of 0.1 mm/s till 32 N load was reached. This load was then held for 30 s, and later released at a rate of 0.1 mm/s. The number of penetrations from the folded parafilm was recorded under a microscope. Classification rules were specified and followed to record the data. They were classified as "holes", "tears", and "dents" as summarised in Fig. 2a-b. "Holes" were penetration points in the parafilm through which the light emitted by the microscope was visible on imaging. "Tears" are penetration points on the parafilm which looked extremely dark, either by tearing and the tear overlapping on itself, or was close to penetration but the elasticity of the parafilm did not allow tearing. Finally, "dents" were classified as points on the parafilm that imprinted a mark on the parafilm, causing minimal stretching.

Histological analysis of microneedle dissolution in murine skin tissue

Skin excisions were taken from sacrificed female mice (20–25 g) following a published protocol (Marwah et al. 2022). Briefly, the hair was removed from the dorsal portion with an animal hair clipper. Using a scalpel and isopropyl alcohol, the dermal fat was removed from the harvested whole thickness skin. All animal experiments are carried out using procedures approved by the Aston University Ethical Review Committee (UK Home Office Licence Number 3003453) in accordance with the 'Guidance on the operation of Animals'

Fig. 2 Microneedle penetration testing using the TA Electroforce 3200 observed PVA 67,000 either with or without trehalose was best able to penetrate the parafilm. Example image of (**a**) layer 1 and (**b**) layer 6 of the 8 layers of parafilm microneedles were pushed through showing holes, tears and dents. "Holes", labelled 'i', are defined as penetration points through which the light emitted by the microscope passes clearly. "Tears", labelled 'ii', are penetration points on the parafilm that look dark due to tearing and overlapping or significant. "Dents", labelled 'iii', are grey spots with small stretch marks with no potential tears. (**c**) The Number of needle penetrations per parafilm layer is plotted for microneedle formulations of PVA 27,000 with trehalose, PVA 67,000 and PVA 67,000 with trehalose. Results are expressed as mean ± standard deviation and analysed by One-way matched pairs ANOVA. $n = 9$ independent batches with 3 repeats each. *$p < 0.05$, **$p < 0.01$, ***$p < 0.001$, ****$p < 0.0001$
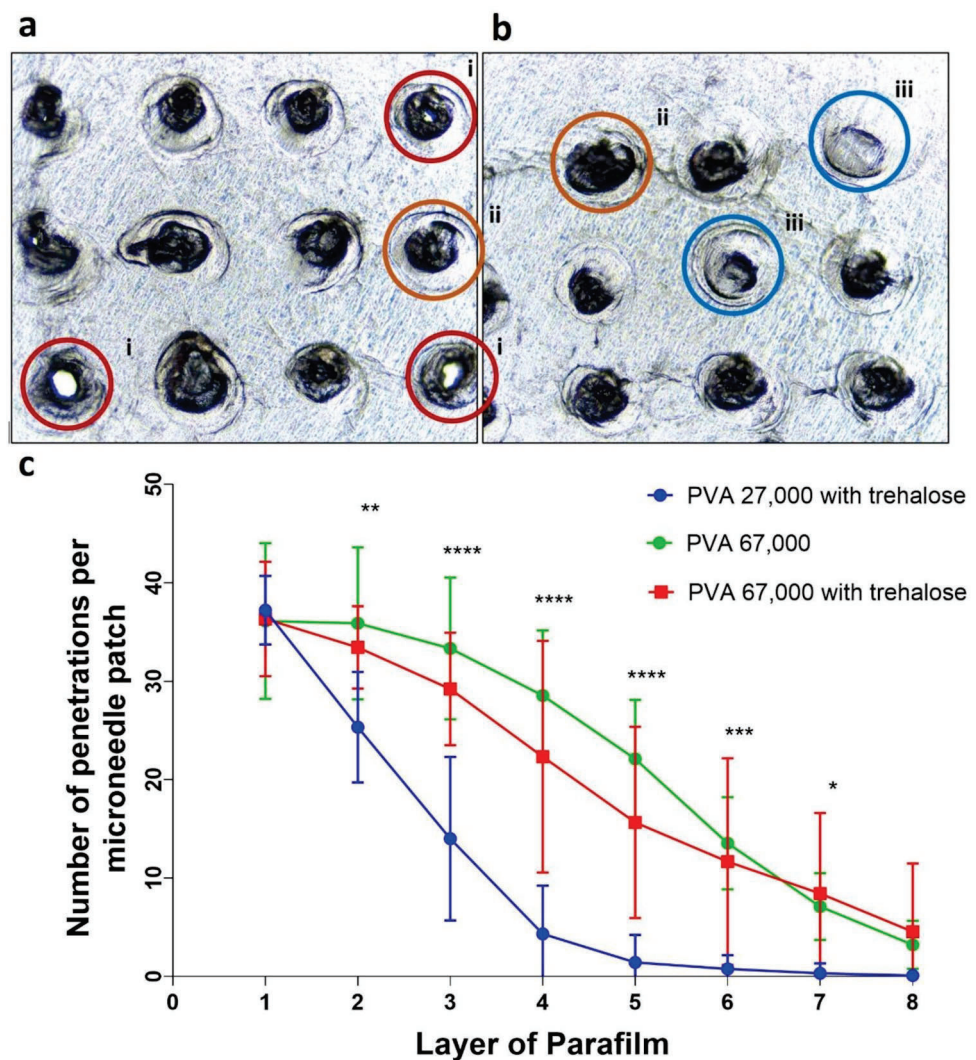
under the United Kingdom Animals (Scientific Procedures) Act 1986.

Microneedles prepared with DilC were prepared to aid histological imaging. These were pressed into the skin excises. After 5 min, base plate was removed, and the murine skin immersed in 4% paraformaldehyde solution for 1 h and then transferred to 30% sucrose solution and finally embedded in Optimal Cutting Temperature compound and stored in -80 °C until further analysis. The skin was then sliced at a 12 µm thickness at -22 °C using the cryostat (Leica CM1950; Nussloch, Germany). Slices were mounted using mounting medium + DAPI (Vectashield) and photographed using a Nikon Eclipse Ti-E inverted microscope (Tokyo, Japan).

Microneedle AP39 release study and dermal accumulation on excised murine skin

For the in vitro assessment of the microneedle's ability to penetrate murine skin, release AP39 and allow AP39 to permeate across, Franz diffusion cells (PermeGear, Hellertown, PA, USA) were used. The system was set up as described in detail previously (Marwah et al. 2022) briefly murine skin (epidermis layer of average thickness 0.31 ± 0.02 mm) samples were cut, washed, and mounted on to the Franz cell receptor immediately after excision. The receiver compartment was filled with phosphate-buffered saline (PBS): ethanol (80:20) and allowed to equilibrate for 30 min, following, a microneedle patch was applied to the skin. At appropriate time intervals, 200 µl of the receptor medium was withdrawn, and the same volume of fresh buffer solution was replaced to the receptor chamber. The concentration of the samples was assayed with HPLC-UV. Following the release study, excised skin was removed from the Franz cell and rinsed 3 times in PBS. Samples were cut and weighed (≤ 30 mg) and immersed in 500 uL acetonitrile containing ceramic beads. Tissue was homogenised with an automatic homogeniser (automatic VelociRuptor V2 Microtube Homogeniser) at room temperature. Samples were removed and centrifuged at 16,000 RCF from which AP39 concentration in the supernatant samples was assayed with HPLC-UV.

A reverse phase HPLC-UV method was used to detect AP39 as described previously (Marwah et al. 2023). Briefly, a Shimadzu LC-2030 C Plus RoHS - Prominence-I separation module HPLC with UV detection was used, at 435 nm operating wavelength. A 10 µL sample was injected at 27 °C into a Phenomenex HyperCloneTM column (5 µm C18 4.6×150 mm column) for analysis. Acetonitrile and 0.05% TFA were mixed in water at a flow rate of 1.25 mL/min to make up the mobile phase in a 64:36 ratio.

Microvascular endothelial model

Primary Human Umbilical Vein Endothelial cells (HUVEC, PromoCell, Cat. # C-12203) were cultured in full growth media (EGM-2) (PromoCell, Cat. # C-22211) supplemented with Fetal Calf Serum 0.02 mg/mL, Epidermal Growth Factor 5ng/ml, Basic Fibroblast Growth Factor 10 ng/ml, Insulin-like Growth Factor 20 ng/mL, Vascular Endothelial Growth Factor 0.5ng/mL, Ascorbic Acid 1 µg/mL, Heparin 22.5 µg/mL, Hydrocortisone 0.2 µg/mL (supplement kit, Promocell, Cat. # C-39211) and 5 mL of 1X Penicilin/Streptomycin (Lonza, Cat. # LZDE17-602E). Culture medium was changed every 48 h and cells were incubated at 37 °C in a 5% CO_2 humidified atmosphere incubator. Cells were subcultured at 70–80% confluency and used for experiments up to passage 5. Before each treatment cells were starved using 5% FBS (Gibco, Cat. # 11550356) M199 starvation media (Lonza, Cat. # LZBE12-119 F) supplemented with antibiotics for 2 h. To ensure the quiescent state of the cells and consistent results, treatments were diluted in the starvation media unless otherwise stated.

HUVEC cells were seeded (3×10^5/ml) on to 24-well polycarbonate inserts (Dias et al. 2015) and cultured for 4 days. On the fifth day tight-junction formation was enhanced through the addition of 250 µM cAMP, 17.5 µM RO 20–1724 and 550 nM hydrocortisone in the absence of serum for 24-hours prior to the initiation of an assay (Elbakary and Badhan 2020). Barrier integrity and formation was assessed through the determination of the trans-endothelial electrical resistance (TEER), which was measured at day 3 and day 4 using a chop-stick electrode (World Precision Instruments STX2).

Drug transport assay

HUVEC cells were grown on permeable inserts and placed into a 24-well cell culture plate. Permeate collected from the Franz cell study was collected, diluted 1 in 4 with serum free culture media and added to the apical compartment with sampling taking place from the basolateral compartment, between 30 and 90 min and replaced with equal amounts of serum free culture medium. AP39 concentrations were analysed using the HPLC method described above. The apparent permeability (P_{app}) was calculated using the equation below,

$$P_{app} = (dQ/dt)/C_0 \times A$$

where dQ/dt the amount of drug permeated per unit time, calculated from the regression line of time points of sampling, C_0 the initial drug concentration in the donor compartment and A is the insert surface area (0.33 cm^2).

Oxidative stress measurement

To explore the potential of AP39 in abrogating oxidative damage induced by H_2O_2, we conducted two assays. First, we explored 8-hydroxy-2′-deoxyguanosine (8-OHdG) immunoreactivity by immunocytochemistry using antibodies against 8-OHdG (Abcam, ab62623). Then, we measured protein carbonyl as a biomarker of oxidative damage to protein with a colorimetric assay using the protocol of the Protein Carbonyl Colorimetric Assay Kit (Cayman Chemical, 10005020). For both assays, SHSY-5Y cells were plated in 12-well plates or coverslips (200 K cells per coverslip) and left to attach overnight. The following day, cells were exposed to 300 μM of H_2O_2 for one hour (Sanchez-Aranguren et al. 2021). Following, cells were washed with warm PBS and exposed to AP39 300 nM for 18 h. After treatments, coverslips were washed in warm PBS and either fixed in cooled ethanol for 5 min or harvested for protein extraction. For the immunocytochemistry, coverslips were permeabilised in 0.15% triton X-100, blocked in 10% goat serum blocking buffer for 1 h and incubated with first antibodies against 8-OHdG (1:100) (overnight), followed by Alexa fluor (488) conjugated secondary antibodies (Abcam, UK, catalogue # ab175658, 1:500). Coverslips were mounted in glass slides using SlowFade TM Diamond Antifade Mountant (Thermo Fisher Scientific, UK). Staining was visualised using a Nikon Eclipse Ti-E inverted microscope using 60× objective lens.

Western blot

To measure cellular neurodegeneration and examine the ability of AP39 to alleviate neurodegeneration, we conducted Western Blot to quantify the level of protein tau, a biomarker of neurodegeneration. Briefly, SHSY-5Y cells were cultured in 6-well plates until confluent. The cells were then exposed to 300 μM of H_2O_2 for one hour and exposed to AP39 300 nM overnight as above. Then, the cells were harvested for protein extraction using RIPA buffer with protease/phosphatase inhibitor (Merck, PPC1010), 0.5 mM phenylmethylsulfonyl fluoride (Merck, 93482), 0.5 mM sodium orthovanadate (Merck, 567540), and 5 mM sodium betaglycerophosphate (Merck, 50020). Protein concentration was quantified using QuantiPro BCA Assay Kit (Merck, QPBCA) and made up in protein loading buffer (National Diagnostics, NAT1252). Protein was then loaded onto a 4–15% polyacrylamide gel and electrophoresis was performed at 150 V for one hour in Tris-Glycine running buffer (National Diagnostics, NAT1218). Then, protein was transferred onto PVDF membrane (Thermo Scientific, 10617354) by electrophoresing at 250 mA for 75 min in Tris-Glycine electroblotting buffer (National Diagnostics, NAT1242). The blot was then blocked in StartingBlock blocking buffer (Thermo Scientific, 37542) before incubation in the primary antibody against tau (1:5000) overnight (Proteintech, 66499-1-Ig). The following day, blots were washed in TBS-Tween and incubated in HRP-conjugated Affinipure Goat Anti-Rabbit IgG (1:1000) for 2 h (Proteintech, SA00001-2). After another wash, protein was visualized using SuperBlot ECL Western Blotting substrate kit (HelloBio, HB9308). The blots were then stripped and re-probed for loading control with primary antibody against β-actin (1:5000) (Proteintech, 66009-1-Ig).

ELISA

The quantification of human IL-6, IL-8 and TNFα in SHSY-5Y cell supernatant was performed using the Human Duo-Set ELISA (DY202, DY208, DY210) from R&D Systems, Abingdon, UK and performed according to the manufacturer's specifications. Briefly, SHSY-5Y were plated in 96-well plates at cell density of 2.0×10^4 cell/well and allowed to attach overnight. As in Sect. 2.9, cells were exposed to H_2O_2 (300 μM) washed with PBS and exposed to AP39 300 nM for 18 h. Afterwards, media was collected and stored at −80 °C until the assay was performed.

Statistical analysis

The results are reported as mean ± standard deviation (SD). The outcomes of the study were statistically analysed using Graphpad Prism version 9.4.1. (La Jolla, CA, USA). Unpaired t-tests, and one- and two-way ANOVA with post-hoc analyses were used to test the data, where $p < 0.05$ was considered significant.

Results

Microneedle characterisation

The formation of microneedles was confirmed using scanning transmission electron microscope (STEM) imaging (Fig. 3). Microscopic inspection of the microneedle arrays revealed conical shaped microneedles were indeed formed at 1305.5 ± 112.83 μm height and 371.13 ± 14.31 μm width (at the base) for PVA 27,000, 1527 ± 65.11 μm height and 343.47 ± 20.58 μm width for PVA 67,000, 1527 ± 71.54 μm height and 282.84 ± 28.43 μm width for PVA 27,000 + trehalose, and 1418.5 ± 68.86 μm height and 384.05 ± 23 μm width for PVA 67,000 + trehalose. The incomplete morphology observed particularly in Fig. 3c is likely due to variations in the fabrication process.
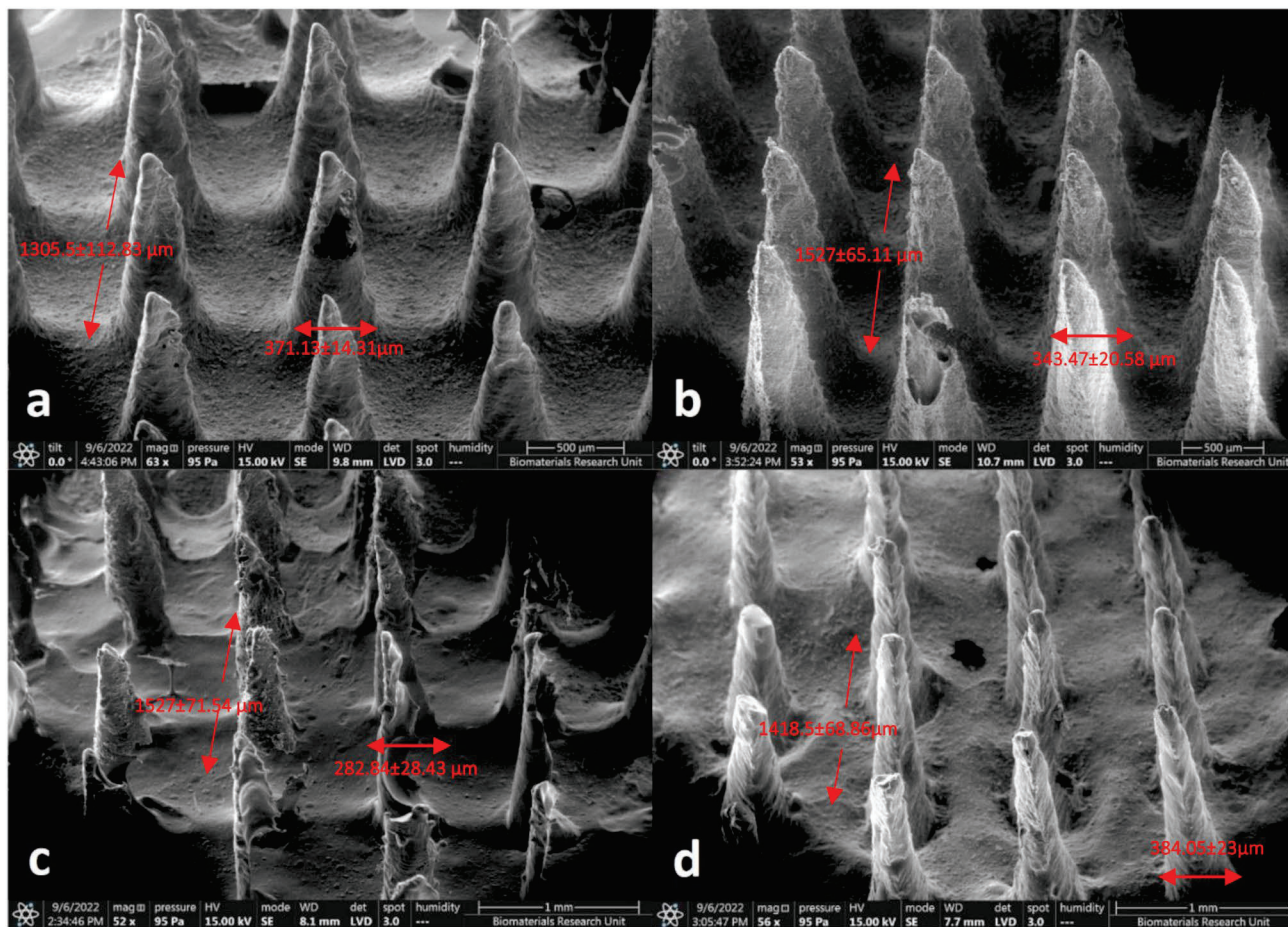
Fig. 3 Microneedle STEM imaging for microneedles produced from the negative moulds using (**a**) PVA 27,000 (**b**) PVA 67,000 (**c**) PVA 27,000 with trehalose (**d**) PVA 67,000 with trehalose. Microneedles were prepared by mixing the polymer and adding the trehalose if required at a final concentration of 20% and 15% w/v respectively. This was poured into the mould, centrifuged and dehydrated following which, the microneedles were removed from the mould and imaged

Microneedle mechanical testing

In order to ascertain properties of the microneedle formulation describing their mechanical strength, the load displacement data was recorded and plotted as shown in Supplementary Fig. 2. From the recorded load per displacement data, the initial break force (load shoulder), hold displacement, and stiffness of the microneedles generated from the four polymer formulations was measured and analysed. As indicated in Supplementary Fig. 2a, the initial break force is the peak load force (N) at the initial shoulder in the load-displacement curve and is indicative of brittleness in the microneedles. The stiffness was recorded as the load displacement slope (N/mm) near the end of the compression stage which is representative of the formulation's resistance to deformation. Finally, the hold displacement is the length of the microneedle undergoing compression (mm) while the 32 N load force is maintained and is indicative of the creep behaviour, i.e., the tendency of a solid material to undergo slow deformation while subject to persistent mechanical stress.

A non-statistically significant higher initial break force was observed in microneedles formulated with PVA 27,000 compared to PVA 27,000 + trehalose with average loads of 5.14 ± 4.39 N and 2.73 ± 1.77 N respectively (Fig. 4a). This appears to show increased brittleness with the addition of the trehalose sugar. However, this pattern was not found between average initial break force of microneedles formulated from PVA 67,000 and PVA 67,000 + trehalose. PVA 67,000 with trehalose values were actually higher than without trehalose with values of 7.59 ± 4.84 N and 7.34 ± 5.79 N respectively however this difference was not statistically significant. Data indicating needle stiffness observed microneedles formulated using PVA 27,000 + trehalose was statistically higher at 185.14 ± 83.47 N/mm compared with PVA 27,000 at 119.46 ± 28.02 N/mm ($p < 0.05$), PVA 67,000 at 78.62 ± 18.86 N/mm ($p < 0.001$) and PVA 67,000 + trehalose at 98.66 ± 29.73 ($p < 0.01$)

Fig. 4 Microneedle fracture testing observed the PVA 67,000 with trehalose formulation was best able to withstand compression force applied by the TA Electroforce 3200. (**a**) Initial break force data, (**b**) stiffness data, (**c**) holding displacement data. Microneedles were prepared by mixing the polymer and adding the trehalose if required at a final concentration of 20% and 15% w/v respectively. This was poured into the mould, centrifuged and dehydrated following which, the microneedles were removed from the mould. Results are expressed as mean ± standard deviation and analysed by one-way ANOVA. $n = 8$ independent batches with 3 repeats each. ***$p < 0.001$, **$p < 0.01$, *$p < 0.05$
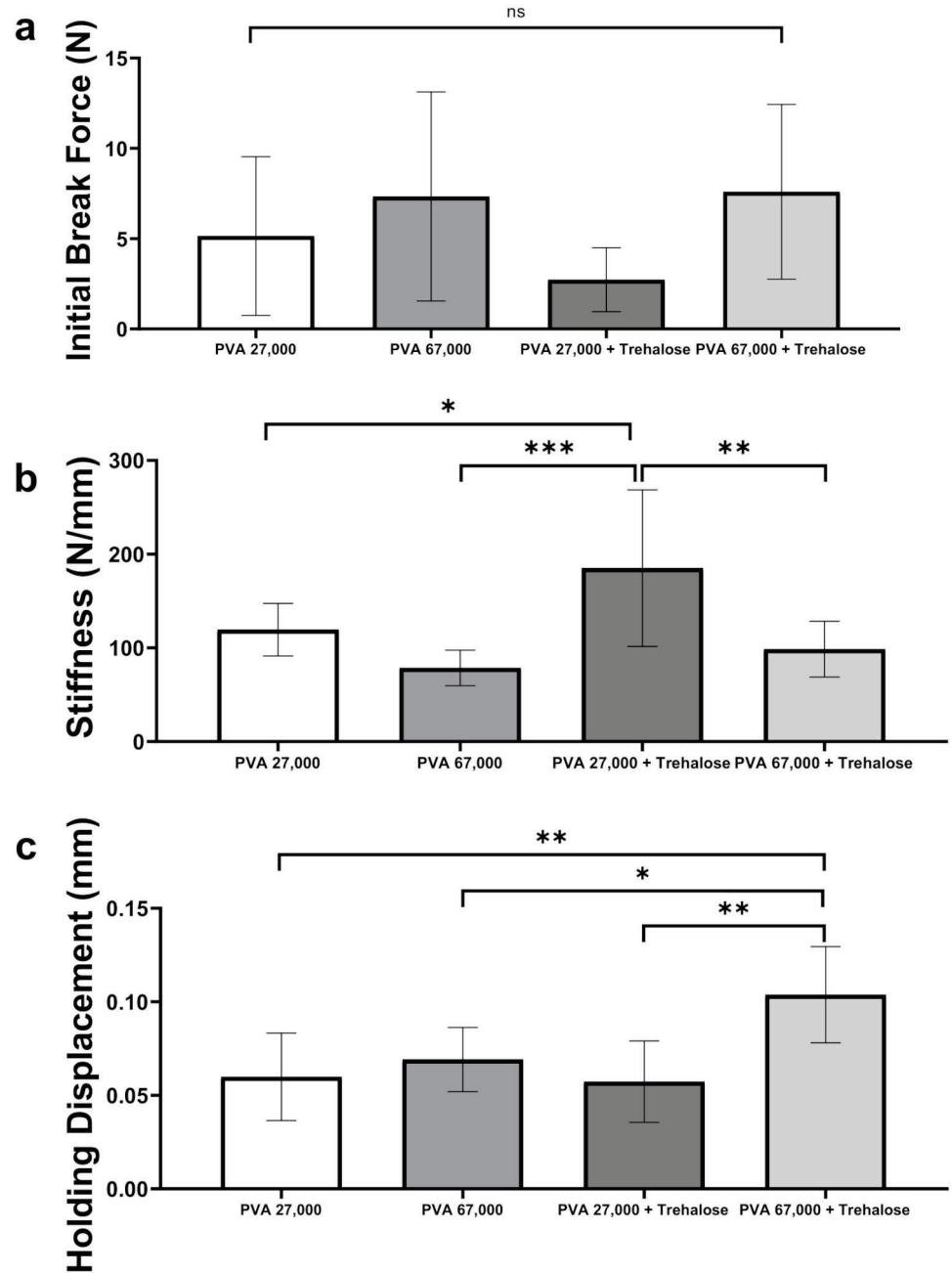
(Fig. 4b). Finally, data determined microneedles formulated from PVA 67,000 + trehalose had the highest holding displacement at 0.104 ± 0.026 mm compared with PVA 27,000 at 0.060 ± 0.023 mm ($p < 0.01$), PVA 27,000 + trehalose at 0.057 ± 0.022 mm ($p < 0.05$) and PVA 67,000 at 0.069 ± 0.017 mm ($p < 0.01$) (Fig. 4c). This indicates the PVA 67,000 + trehalose formulation was best able to withstand the applied mechanical stress.

Penetration test

The penetration of the microneedles into 8 layers of parafilm was recorded. All holes and tears were included for analysis in Fig. 2c. PVA 27,000 was excluded for all remaining studies owing to their unsatisfactorily properties thus far. Microneedles formulated PVA 27,000 + trehalose observed the lowest penetration across the parafilm layers. Incidences of holes and tears were statistically higher in microneedles formulated from PVA 67,000 ($p < 0.05$) and PVA 67,000 + trehalose ($p < 0.01$). The difference in penetration

was not statistically significant between microneedles formulated from PVA 67,000 and PVA 67,000 + trehalose.

Further comparisons were made in penetrations observed between each parafilm layer across the formulations. In layer 3, comparing the number of needle penetration for PVA 27,000 + trehalose, PVA 67,000 and PVA 67,000 + trehalose was 14.00 ± 8.31, 33.33 ± 7.21 and 29.22 ± 5.72 ($p < 0.0001$). Similarly for layer 4, it was 4.33 ± 4.90, 28.56 ± 6.62 and 22.33 ± 11.76 ($p < 0.0001$). For layer 5 it was, 1.44 ± 2.79, 22.11 ± 5.99 and 15.67 ± 9.72 ($p < 0.0001$). Starting from layer 6, there was a diminishing statistical significance, and by layer 8, no discernible distinction was noted. Based on both the mechanical testing and penetration outcomes of microneedles, those composed of 67,000 + trehalose were chosen for further examination.

Microneedle penetration and flux of AP39 across excised murine skin

Studies were performed to evaluate the ability of microneedle formulations arrays to penetrate through the excised murine skin. Microneedles, loaded with DilC, were able to successfully pierce murine skin as highlighted in Fig. 5a. Permeation of AP39 through ex vivo samples of murine skin were assessed (Fig. 5b). Following 32 h after the applications of the AP39 microneedles as well as a baseplate consisting of the same formulation with no microneedles observed $32.84 \pm 2.11\%$ compared with 0% of AP39 permeated across the excised murine skin. Following 24-hours, skin was wiped clean and accumulation of AP39 in ex vivo skin samples measured (Fig. 5c). Results showed that the microneedle preparation observed a higher accumulation of AP39 within the skin at $49.93 \pm 4.70\%$ compared with the baseplate showing only $3.66 \pm 2.06\%$ within the skin

($p < 0.0001$) suggesting the AP39 in the baseplate was not successfully able to permeate into the skin.

Microvascular endothelial model and AP39 permeability assay

The formation of a high resistance barrier was determined by measuring the trans-endothelial electrical resistance (TEER) values from monolayers of HUVECs' grown on permeable inserts (Fig. 6a). The effect of endothelial tight junction inducing agents exposed to cells for 24 h on day 4 post seeding was determined. On day 4, TEER values significantly increased from to $72.19 \pm 2.87 \ \Omega.cm^2$ to $146.00 \pm 7.74 \ \Omega.cm^2$ ($p < 0.0001$) (Fig. 6a). The permeability of AP39 across HUVECs that were grown on permeable inserts was determined (Fig. 6b). Over 90 min, 6.06 ± 0.17 mcg/mL permeated across, giving an apparent membrane permeability (P_{app}) of $18.61 \pm 1.40 \times 10^{-6}$ cm/s.

Impact of AP39 on oxidative stress

8-hydroxy-2-deoxyguanosine (8-OHdG) immunoreactivity, an index of oxidative DNA damage, was profoundly increased in cells exposed to H_2O_2 compared to control group (Fig. 6c). We observed that administration of AP39 (300 nM) attenuated H_2O_2-induced oxidative stress as indicated by decreased 8-OHdG immunoreactivity in cells exposed to both, H_2O_2 and AP39. Protein carbonyl content is a widely used biomarker for oxidative stress, reflecting extent of protein oxidation within cells. Elevated levels of protein carbonyls indicate increased oxidative damage, a hallmark of pathological conditions including neurodegenerative diseases. In this study, there was a significant difference in protein carbonyl content ($p < 0.01$) with an expected
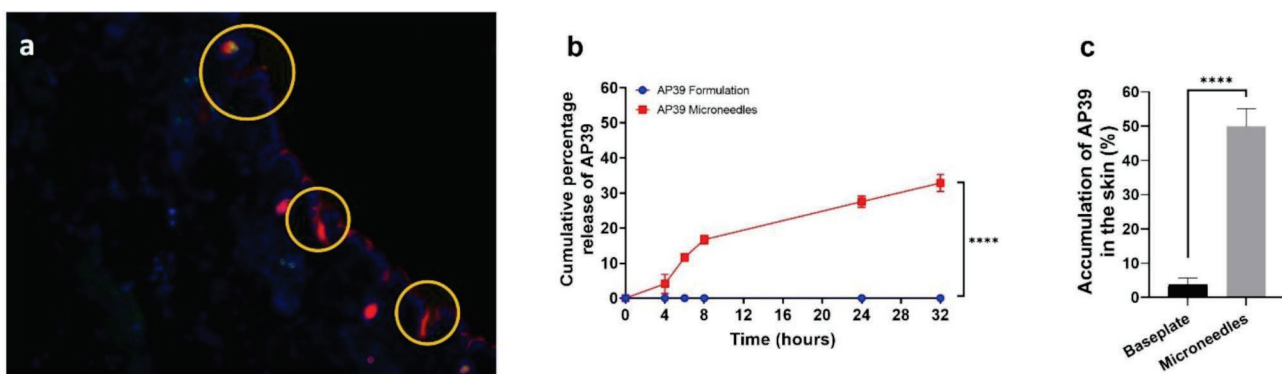

Fig. 5 Microneedles formulated with PVA 67,000 with trehalose increased AP39 flux across ex-vivo murine skin samples and increased accumulation within the skin compared to a microneedle baseplate with no needles. (**a**) histology of ex vivo skin following application of microneedles formulated with DilC (red), cell nuclei were visualized using DAPI (blue) (**b**) Cumulative percentage AP39 release profiles up to 32 h. (**c**) AP39 accumulation in ex-vivo murine skin samples following 24-h application to a 1 cm2 sample of excised skin. Release across skin was observed using a Franz cell system quantified by HPLC-UV analysis. Results are expressed as mean ± standard deviation and analysed by One-way ANOVA. $n = 3$ independent batches with 3 repeats each. ***$p < 0.001$, **$p < 0.01$
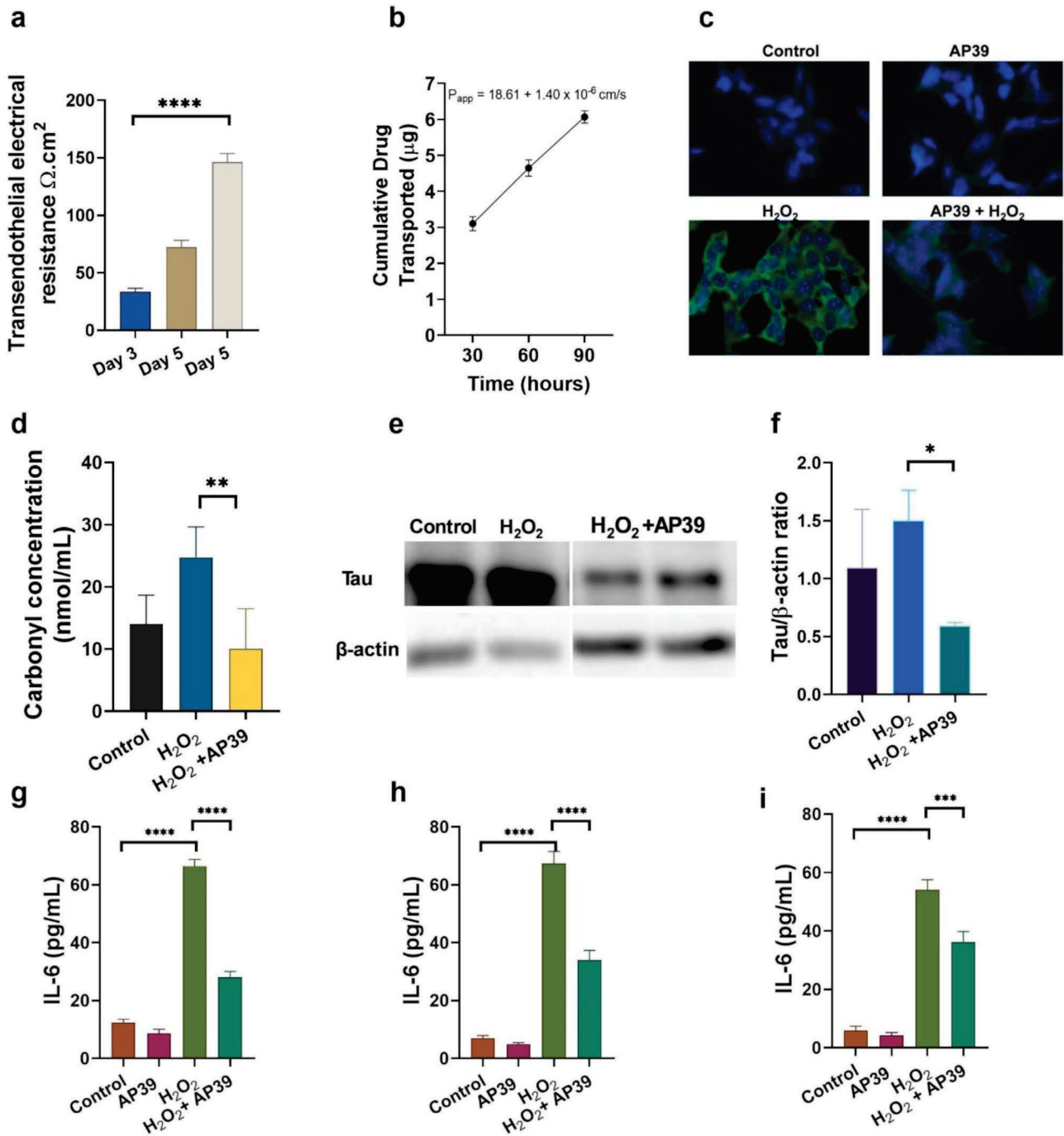
Fig. 6 AP39 permeated across microvascular endothelial model using HUVECs grown on permeable inserts and was able to attenuate H_2O_2-induced oxidative stress and inflammation in SHSY5Y cells. (**a**) TEER values measured following growth of HUVEC cells on permeable cell culture inserts in the absence and presence of tight junction forming additives. (**b**) AP39 transport from apical to basolateral compartment with associated apparent membrane permeability (Papp). (**c**) AP39 attenuates H_2O_2-induced oxidative stress in SHSY5Y cells. Set of representative images depicting anti-8-OH-dG immunofluorescence (green). Blue colour (DAPI) denotes nuclei. H_2O_2 (300 μM) was administered for one hour. Following, media was replaced, cells washed and AP39 (300 nM) administered for 18 h. Images were taken using 60× magnification. (**d**) Carbonyl concentration following H_2O_2 (300 μM) treatment was significantly reduced by AP39 treatment. (**e**) Expression of tau and β-actin assessed by Western Blot in cells exposed to H_2O_2 (1 h), followed by 18 h exposure to AP39. (**f**) Quantification of tau protein expression, relative to β-actin showed significant reduction in tau expression level after AP39 treatment. (**g**) IL-6, (**h**) IL-8 and (**i**) TNFα release measured by ELISA in cell culture media. * $p < 0.05$, *** $p < 0.001$, ****$p < 0.0001$. $n = 4$ independent experiments with 6 repeats each

increase in protein carbonyl concentration from a baseline (control) value of 14.01 ± 2.08 nmol/mL to a H_2O_2-treated value of 24.75 ± 2.19 nmol/mL (Fig. 6d). Treatment with AP39 significantly ($p < 0.01$) reduced the protein carbonyl concentration to a value of 10.00 ± 2.90 nmol/mL. This suggests that AP39 exhibited potent effect in suppressing oxidative stress following H_2O_2 insult in the cells.

Western blot analysis of tau protein to assess neurodegeneration and AP39 efficacy

To measure the burden of neurodegeneration in the cells and examine the capacity of AP39 to alleviate neurodegeneration, we conducted Western Blot to quantify the level of protein tau, a well-established biomarker of neurodegeneration. There was a significant difference in the tau/β-actin ratio ($p < 0.05$), indicating changes in the level of tau in the cells (Fig. 6e and f). H_2O_2 treatment induced an expected accumulation of tau ratio from a baseline (control) value of 1.09 ± 0.29 to 1.50 ± 0.15. Treatment with AP39 significantly ($p < 0.05$) reduced tau ratio in the cells to a value of 0.59 ± 0.02. This indicates the effect that AP39 has on inhibiting tau accumulation in the brain cells.

Anti-inflammatory potential of permeated AP39 on inflammatory cytokines IL-6, IL-8, and TNF-α

The determination of levels in SHSY-5Y tissue culture media indicated that exposure of H_2O_2 significantly stimulated the release of IL-6, IL-8, and TNF-α in (66.48 ± 2.33, 67.41 ± 4.13 and 54.09 ± 3.45 respectively) ($p < 0.0001$, Fig. 6f-h). However, treatment with AP39 significantly reduced the release of IL-6, IL-8, and TNF-α (28.11 ± 1.92, 33.90 ± 3.45 and 36.10 ± 3.72 respectively) ($p < 0.0001$, $p < 0.0001$ and $p < 0.001$ respectively).

Discussion

Despite the development of many H_2S donors, few have progressed to clinical application. The main obstacle lies in effectively delivering H_2S at a controlled rate to ensure optimal bioavailability within the therapeutic range and minimising potential toxicity. Our research efforts yielded a transdermal microneedle patch that exhibits favourable mechanical properties and material strength, enabling effective penetration of the skin. Furthermore, we demonstrated sustained release capabilities and observed the desired pharmacological effect of the drug in SHSY5Y cells, providing compelling evidence for its efficacy. The delivery system we have developed effectively overcomes significant challenges associated with drug administration, including the

necessity for repeated doses, drug instability, and losses due to first-pass metabolism typically observed in oral delivery methods. Additionally, this system obviates the requirement for professional administration typically associated with intravenous routes, eliminates the presence of biohazardous sharps, and ensures a patient-friendly approach.

A wide range of polymers have been used to fabricate dissolving microneedle arrays, PVA is one such polymer owing to its ability to withstand the required force to penetrate the skin whilst having a rapid dissolution once embedded into skin (Moore et al. 2022). The mechanical strength of the PVA microneedles produced from two different molecular weights both with and without trehalose was investigated. The initial break force was used to measure the brittleness of the material. There was a trend in the PVA with a greater molecular weight having a larger initial break force as compared to the lower molecular weight. In a comparable study where PVP of several molecular weights was used to create microneedles, a similar trend was observed where the baseplates of the smaller molecular weight PVP formulations were too brittle thus replaced with a higher molecular weight PVP (Thakur et al. 2016). This may be due to the lower molecular weight PVA 27,000 having lower intermolecular forces as compared to PVA 67,000 (Sun et al. 2008). The addition of trehalose showed a decreasing trend in the initial breaking force in the case of PVA 27,000 suggesting the trehalose tends to make the formulation more brittle. This effect was explored in a study by Raphael, et al., (2016) where the increase in addition of trehalose to carboxymethylcellulose microneedles (from a 1:1 ratio to 30:1) made the microneedles more brittle. They also observed a reduction of the elastic modulus of the formulation suggesting the presence of trehalose introduced pockets of crystalline regions interfering with the carboxymethylcellulose matrix. It's noteworthy that they found the macroscopic features, such as brittleness or malleability, did not dictate the microscopic characteristics, like crystalline or amorphous structures, in terms of transdermal penetrability. Furthermore, according to Thakur, et al., (2016) to ensure similar mechanical strengths when creating microneedles of different molecular weights, a decreasing ratio of sugar to polymer formulation was added when increasing the carboxymethylcellulose molecular weight. This might explain why PVA 27,000 showed an increase in stiffness when formulated with trehalose whereas no such change was found in the PVA 67,000 formulation. Further exploration of different polymer molecular weights as well as trehalose loadings may provide further insight into the mechanical properties of each material.

Stiffness refers to an elastic body's ability to resist deformation when subjected to an external force. Consistent with prior research where trehalose supplementation enhanced

the stiffness of the material, thus reinforcing pullulan microneedles (2022), a similar effect was observed when trehalose was incorporated into PVA 27,000, resulting in heightened microneedle stiffness. Furthermore, our study revealed that PVA 27,000 exhibited increased stiffness and brittleness, indicated by a reduced initial break force, compared to PVA 67,000. This is similar to Thakur et al's study (41) where PVP of different molecular weights were compared, with the high molecular weight PVP K29/32 forming the least brittle microneedle array, and low molecular weight PVP K15 producing the most brittle microneedle array. PVA 67,000 with trehalose had the largest holding displacement (creep) and the highest initial break force (compressive strength) suggesting this formulation gave the strongest needles of the formulations investigated. A similar study observing the mechanical strength and shape-stability of hydrogels found that increasing the molecular weight of PVA increases the compressive strength (2010) with the addition of trehalose further increasing formulation strength (Tian et al. 2022).

Formulation penetration testing observed microneedles formulation with PVA 67,000 both with and without trehalose showed deeper penetration was superior to PVA 27,000. This may be owing to the brittleness of the microneedles formulated with PVA 27,000 causing the sharp needle tips to break off, leaving a thicker needle base that will limit ability to penetrate the skin. Microneedles formulated from PVA 67,000 and trehalose were used to proceed with analysing the microneedle design for further study. Similar to previous microneedle studies, the histological analysis for microneedle formulated from PVA 67,000 + trehalose showed needles were able to break through the skin and deposit the drug (Khosraviboroujeni et al. 2022). Finally, the microneedle formulation allowed drug to permeate across the skin and into the release media compared with baseplate alone where no drug permeation was observed. Taken together, results show that despite the incomplete morphology observed in images—potentially influenced by fabrication conditions—the microneedles are strong enough for transdermal drug delivery and successful in delivering AP39. Furthermore, drug accumulation in the skin was markedly higher than with the baseplate formulation alone, considering no drug permeated across the skin, it may be assumed that drug deposition only occurred in the upper layers of the skin and was not able to permeate beyond this. Although drug penetration through murine skin may differ from that in human tissue, the latter is not readily available. Murine skin is a widely used alternative (Jung et al. 2020; Fang et al. 2009; Zhu et al. 2016) with some compounds permeating in a similar manner, whereas others differ in drug release owing to human skin being less permeable (Simon and Maibach 1998). Further work is required to establish the drugs kinetic profile thought human skin.

Development of drug treatments for delivery to the central nervous system is particularly challenging due to the presence of the blood-brain barrier. The blood-brain barrier separates the systemic circulation from the cerebral parenchyma and is composed of cerebral capillary endothelial cells connected by tight junctions which contribute towards reduced permeation of small-molecule drugs permeability (Temsamani et al. 2000). This study observed AP39 collected from the receiver compartment from the skin permeation study was able to permeate across a cellular barrier model. Previous studies have observed that when AP39 was delivered to mice, an increase in H_2S levels in the brain cortex was observed. Further studies are required to elucidate the precise mechanism of AP39 crossing the blood-brain barrier. Finally, permeated drug was able to reduce oxidative stress and inflammation on neuronal cells. Previously, it has been shown that AP39 restores the mitochondrial function and ameliorates oxidative stress induced by H_2O_2 (Sanchez-Aranguren et al. 2021, Szczesny et al. 2014; Zhao et al. 2016; Marwah et al. 2023). Protein carbonyl is a well-established biomarker of oxidative stress (Dalle-Donne et al. 2003). Our study showed H_2O_2 produced cellular oxidative stress, resulting in oxidative damage to proteins and formation of protein carbonyl. AP39 treatment significantly reduced protein carbonyl level, indicating its potent antioxidant activity. Furthermore, oxidative stress is known to promote tau accumulation (Haque et al. 2019), a hallmark of various neurodegenerative diseases (Gao et al. 2018). We observed H_2O_2 treatment increased the level of tau in the cells whilst AP39 treatment exhibited potent inhibition in tau accumulation, consistent with previous reports of its beneficial effect in preventing neurodegeneration (Zhao et al. 2016). The reduction in IL-6 is also particularly noteworthy, given its role in chronic inflammation and neurodegenerative diseases (Shan et al. 2024). Similarly, the decreased levels of IL-8 and TNF-α further support the anti-inflammatory properties of AP39, as these cytokines are critical mediators in the inflammatory response. Our results are consistent with these previous reports and suggest that transdermal microneedle formulations of AP39 retain the protective role of AP39 in abrogating oxidative stress and reducing inflammation. The strong inhibitory effect that AP39 has on tau accumulation also demonstrates its therapeutic potential to alleviate neurodegeneration. In vivo testing is required to validate these results and confirm the effectiveness of AP39 in a physiological context, as well as to fully understand its mechanisms of action in crossing the blood-brain barrier and exerting neuroprotective effects.

Conclusion

The transdermal delivery of AP39 represents a promising and non-invasive therapeutic approach with significant potential for treating neurological disorders. This method offers the potential of maintaining sustained drug levels in the bloodstream, thereby minimising both toxicity and the frequency of dosage. To achieve this, a technique for producing dissolving microneedles was employed, utilising 3D printing to create a unique needle mould. Microneedles made from varying molecular weights of PVA, both with and without trehalose, were successfully generated through this method. Notably, microneedles composed of PVA 67,000 with trehalose exhibited the necessary strength to penetrate the skin and deliver the drug across the skin. The drug permeated the skin, crossed a microvasculature model, and effectively reduced oxidative stress and inflammation in neuronal cells, demonstrating its potential to enhance neuronal cell health and improve clinical outcomes in neurological disorders. Therefore, the development of a systemic delivery method for H_2S donors like AP39 via skin application appears to be a practical and feasible approach to drug administration.

Declarations

Statement of animal rights All animal experiments were carried out using procedures approved by the Aston University Ethical Review Committee (UK Home Office Licence Number 3003453) in accordance with the 'Guidance on the operation of Animals' under the United Kingdom Animals (Scientific Procedures) Act 1986.

Conflict of interest All authors (P. Balakrishnan, S. Junaid, S. Ahmad, K. Wang, Y.S. Hindalekar, H. Shokr, M. Upadhya, S. Hopkins, J. Sacharczuk, K. Singh Rana, M. Anas Al Tahan, P. Juvale, F. Chan, L. Sanchez-Aranguren, and M. Marwah) declare that they have no conflict of interest.

References

Alkilani AZ, Mccrudden MT, Donnelly RF (2015) Transdermal Drug Delivery: innovative Pharmaceutical developments based on disruption of the Barrier properties of the stratum corneum. Pharmaceutics 7:438–470

Amor S, Puentes F, Baker D, van der Valk (2010) Inflammation in neurodegenerative diseases. Immunology 129:154–169

Caliendo G, Cirino G, Santagada V, Wallace JL (2010) Synthesis and Biological effects of Hydrogen Sulfide (H2S): development of H2S-Releasing drugs as pharmaceuticals. J Med Chem 53:6275–6286

Checkoway H, Lundin, J. I., Kelada SN (2011) Neurodegenerative diseases. IARC Scientific, 407–19

Dabbagh SR, Sarabi MR, Rahbarghazi R, Sokullu E, Yetisen, A. K., Tasoglu S (2021) 3D-printed microneedles in biomedical applications. iScience 24:1–22

Dalle-Donne I, Giustarini Rossir, Milzani D, A., Colombo R (2003) Protein carbonyl groups as biomarkers of oxidative stress. Clin Chim Acta 329:23–38

Dias HK, Brown CL, Polidori MC, Lip, G. Y., Griffiths HR (2015) LDL-lipids from patients with hypercholesterolaemia and Alzheimer's disease are inflammatory to microvascular endothelial cells: mitigation by statin intervention. Clin Sci (Lond), 129, 1195–206

Dugger BN, Dickson DW (2017) Pathology of neurodegenerative diseases. Cold Spring Harb Perspect Biol, 9

El-Sayed N, Vaut, L., Schneider M (2020) Customized fast-separable microneedles prepared with the aid of 3D printing for nanoparticle delivery. Eur J Pharm Biopharm 154:166–174

Elbakary B, Badhan RKS (2020) A dynamic perfusion based blood-brain barrier model for cytotoxicity testing and drug permeation. Sci Rep 10:3788

Fang Y-P, Huang Y-B, Wu P-C, Tsai Y-H (2009) Topical delivery of 5-aminolevulinic acid-encapsulated ethosomes in a hyperproliferative skin animal model using the CLSM technique to evaluate the penetration behavior. Eur J Pharm Biopharm 73:391–398

Gao YL, Wang N, Cao Sunfr, Zhang XP, W., Yu JT (2018) Tau in neurodegenerative disease. Annals Translational Med 6:175

Gerő D, Perry Torregrossar, Le-Trionnaire Awatersa, Wood Swhatmorejl, M., Whiteman M (2016) The novel mitochondria-targeted hydrogen sulfide (H(2)S) donors AP123 and AP39 protect against hyperglycemic injury in microvascular endothelial cells in vitro. Pharmacol Res 113:186–198

Haque MM, Kim Muraledp, Y. K., Lee JS (2019) Crosstalk between oxidative stress and Tauopathy. Int J Mol Sci, 20

Hu L-F, Lu M, Hu Tiongcxdawegs, G., Bian J-S (2010) Neuroprotective effects of hydrogen sulfide on Parkinson's disease rat models. Aging Cell 9:135–146

Ikeda K, Marutani E, Hirai S, Wood ME, Whiteman M, Ichinose F (2015) Mitochondria-targeted hydrogen sulfide donor AP39 improves neurological outcomes after cardiac arrest in mice. Nitric Oxide, 49

Jellinger KA (2010) Basic mechanisms of neurodegeneration: a critical update. J Cell Mol Med 14:457–487

Jung JH, Jin SG (2021) Microneedle for transdermal delivery: current trends and fabrication. J Pharm Invest 51:503–517

Jung H, Kim MK, Choi Leejy, S. W., Kim J (2020) Adhesive Hydrogel Patch with enhanced strength and adhesiveness to skin for Transdermal Drug Delivery. Adv Funct Mater 30:2004407

Kausar S, Wang F, Cui H (2018) The role of Mitochondria in reactive Oxygen species Generation and its implications for neurodegenerative diseases. Cells, 7

Khosraviboroujeni A, Mirdamadian SZ, Minaiyan M, Taheri A (2022) Preparation and characterization of 3D printed PLA microneedle arrays for prolonged transdermal drug delivery of estradiol valerate. Drug Delivery Translational Res 12:1195–1208

Kima J-Y, Hanb M-R, Kim Y-H, Shin, S.-W., Nam, S.-Y., Park J-H (2016) Tip-loaded dissolving microneedles for transdermal delivery of donepezil hydrochloride for treatment of Alzheimer's disease. Eur J Pharm Biopharm 105:148–155

Krieger KJ, Lowry Bertollondangolmsheridanjt, M. M., O'cearbhaill ED (2019) Simple and customisable method for fabrication of high-aspect ratio microneedle molds using low-cost 3D printing. Microsystems Nanoengineering 5:1–14

Marwah MK, Shokr H, Sanchez-Aranguren L, Wang Badhanrks, K., Ahmad S (2022) Transdermal Delivery of a Hydrogen Sulphide Donor, ADT-OH using aqueous gel formulations for the treatment of impaired vascular function: an Ex vivo study. Pharm Res 39:341–352

Marwah MK, Manhoosh B, Shokr H, Al Tahan MA, Stewart R, Iqbal M, Abdullah Sanchezld, Ahmad S, Wang S (2023) Transdermal delivery of mitochondrial-targeted hydrogen sulphide donor, AP39 protects against 6-hydroxydopamine-induced mitochondrial dysfunction. Eur J Pharm Biopharm 191:166–174.

Moore LE, Vucen S, Moore AC (2022) Trends in drug- and vaccine-based dissolvable microneedle materials and methods of fabrication. Eur J Pharm Biopharm 173:54–72

Nissanka N, Moraes CT (2018) Mitochondrial DNA damage and reactive oxygen species in neurodegenerative disease. FEBS Lett 592:728–742

Raphael AP, Crichton ML, Falconer RJ, Chen Meligas, Huang Xfernandogjp, H., Kendallabe MAF (2016) Formulations for microprojection/microneedle vaccine delivery: structure, strength and release profiles. J Controlled Release 225:40–52

Relja M (2004) Pathophysiology and classification of neurodegenerative diseases. Electron J Int Federation Clin Chem Lab Med 15:97–99

Sanchez-Aranguren L, Marwah, M. K., Nadeem S (2021) Neuroprotective effects of mitochondrial-targeted hydrogen sulphide donor, AP39 on H2O2-induced oxidative stress in human neuroblastoma SHSY5Y cell line. Adv Redox Res 3:100024

Shan C, Zhang C, Zhang CJNR (2024) The role of IL-6 in neurodegenerative disorders. Neurochem Res 49:834–846

Shefa U, Kim MS, Jeong NY, Jung J (2018) Antioxidant and cell-signaling functions of Hydrogen Sulfide in the Central Nervous System. Oxidative Med Cell Longev 2018:1873962

Simon GA, Maibach HI (1998) Relevance of Hairless Mouse as an experimental model of Percutaneous Penetration in Man. Skin Pharmacol Physiol 11:80–86

Singh A, Kukreti R, Saso L, Kukreti S (2019) Oxidative stress: a key modulator in neurodegenerative diseases. Molecules, 24

Sun G, Zhang X-Z, Chu C-C (2008) Effect of the molecular weight of polyethylene glycol (PEG) on the properties of chitosan-PEG-poly(N-isopropylacrylamide) hydrogels. J Mater Science: Mater Med 19:2865–2872

Szczesny B, Yanagi Modisk, Coletta K, Trionnaire C, Perry SL, Wood A, Whiteman ME, M., Szabo C (2014) AP39, a novel mitochondria-targeted hydrogen sulfide donor, stimulates cellular bioenergetics, exerts cytoprotective effects and protects against the loss of mitochondrial DNA integrity in oxidatively stressed endothelial cells in vitro. Nitric Oxide: Biology Chem 41:120–130

Tabassum R, Jeong, N. Y., Jung J (2020) Therapeutic importance of hydrogen sulfide in age-associated neurodegenerative diseases. Neural Regeneration Res 15:653–662

Temsamani J, Rees Scherrmannj, A., Kaczorek M (2000) Brain drug delivery technologies: novel approaches for transporting therapeutics. Pharm Sci Technol Today 3:155–162

Teo AL, Shearwood C, Lu Ngkc, J., Moochhala S (2006) Transdermal microneedles for drug delivery applications. Mater Sci Engineering: B 132:151–154

Thakur RRS, Al-Shammari Tekkoia, Mccarthy Faliaa, H., Donnelly RF (2016) Rapidly dissolving polymeric microneedles for minimally invasive intraocular drug delivery. Drug Delivery Translational Res 6:800–815

Tian Y, Lee J, van der Maaden K, Bhide Y (2022) Intradermal Administration of Influenza Vaccine with Trehalose and Pullulan-based dissolving microneedle arrays. J Pharm Sci 111:1070–1080

Vora LK, Gonzalez-Vazquez Donnellyrflarranetae, P., Thakur, R. R. S., Vavia PR (2017) Novel bilayer dissolving microneedle arrays with concentrated PGLA nano-microparticles for targeted intradermal delivery: Proof of Concept. J Controlled Release 265:93–101

Wang Y, Xu E, Musich, P. R., Lin F (2019) Mitochondrial dysfunction in neurodegenerative diseases and the potential countermeasure. CNS Neurosci Ther 25:816–824

Zhang X, Bian JS (2014) Hydrogen sulfide: a neuromodulator and neuroprotectant in the central nervous system. ACS Chem Neurosci 5:876–883

Zhao F-L, Fang F, Qiao P-F, Gao Yann, D., Yan Y (2016) AP39, a Mitochondria-Targeted Hydrogen Sulfide Donor, Supports Cellular Bioenergetics and Protects against Alzheimer's Disease by Preserving Mitochondrial Function in APP/PS1 Mice and Neurons. Oxidative Medicine and Cellular Longevity, 2016

Zhu DD, Wang, Q. L., Liu, X. B., Guo XD (2016) Rapidly separating microneedles for transdermal drug delivery. Acta Biomater 41:312–319